Comparative assessment of a foam-based oxidative treatment of hydrocarbon-contaminated unsaturated and anisotropic soils

Iheb Bouzid, Julien Maire, Nicolas Fatin-Rouge

Comparative assessment of a foam-based oxidative treatment of hydrocarbon-contaminated unsaturated and anisotropic soils

Iheb Bouzid, Julien Maire, Nicolas Fatin-Rouge*

Université de Bourgogne Franche-Comté − Besançon, Institut UTINAM − UMR CNRS 6213, 16, route de Gray, 25030, Besançon, France

Corresponding author: Nicolas Fatin-Rouge

E-mail: nicolas.fatin-rouge@univ-fcomte.fr

Telephone: + 33-3-81-66-20-91

Abstract:

In situ delivery of liquid reagents in vadose zone is limited by soil anisotropy and gravity. The enhanced delivery of persulfate (PS) as oxidant, using a new foam-based method (F-PS) was compared at bench-scale to traditional water-based (W-PS) and surfactant solution-based (S-PS) deliveries. The goal was to distribute PS uniformly in coal tar-contaminated unsaturated and anisotropic soils, both in terms of permeability and contamination. Water was the less efficiently delivered fluid because of the hydrophobicity of the contaminated soils. Surfactant enhanced PS-distribution into contaminated zones by reducing interfacial tension and inverting soil wettability. Regardless of coal tar contamination contrasts (0 *vs.* 5 and 1 *vs.* 10 $g.kg_{soil}^{-1}$) or strong permeability contrasts, PS-solution injection after foam injection led to the most uniform reagents delivery. While PS-concentration varied more than 5-times between zones using W-PS and S-PS methods, it varied less than 1.6-times when the F-PS one was used. Finally, despite unfavorable conditions, the foam-based method did not show any detrimental effect regarding the oxidation of hydrocarbons compared to the W-PS and S-PS methods carried out in ideal conditions. Moreover, hydrocarbon degradation rates were slightly higher when using F-PS than S-PS due to a lower surfactant content in the targeted zone.

Keywords :

Coal tar contamination ; Vadose zone ; Soil anisotropy ; ISCO ; Surfactant foam

1. Introduction

Persistent organic pollutants (POPs) are hazardous compounds. Their presence in contaminated soils and groundwater often result from spillages. Coal tars are viscous hydrocarbons that contain many POPs such as polycyclic aromatic hydrocarbons (PAHs) [1]. Soils with such contaminations are notoriously difficult to treat because of the contaminants. Indeed, the latter are often tightly bound to soil particles and their release occurs over decades [2]. The *in situ* remediation of contaminated soils is growing, since it reduces the risks associated with contaminants dissemination and hazards [3].

In situ chemical oxidation (ISCO) is one of the most innovative technologies to remove POPs at residual saturations [3–5]. However, its efficiency is limited by the slow desorption of hydrophobic contaminants. The use of surfactants coupled with chemical oxidation (S-ISCO) revealed the improvement of the availability of hydrocarbons [6–10]. However, the treatment efficiency is often hindered by the poor contact between oxidants and contaminants. This is especially true in the vadose zone, where gravity and anisotropy (permeability and hydrophobicity) limit the isotropic distribution of reactants [11,12]. Indeed, traditional water-based fluids in vadose zone are prone to vertical migration, capillary phenomena, such as capillary suction into small pores, and bypassing of hydrophobic contaminated zones.

Currently, there is a growing interest for the use of high viscosity shear-thinning fluids for soil remediation. Among them, surfactant foam has proved to be a promising fluid for *in situ* environmental remediation (ISER) [13–16], especially to deliver remedial amendments [11,17–21]. Surfactant foam in porous media appears as trains of gas bubbles separated by thin liquid films (lamellae) stabilized by surfactant molecules. The lamellae rest at pore throats. They have to stretch to go through pores or break, opposing resistance to gas flow. Foam exhibits advantages of high viscosity, shear-thinning behavior and low-density fluid [22], making its propagation in vadose zone less affected by gravity and anisotropy. However, when carrying out foam-enhanced ISCO, the

simultaneous presence of surfactant and oxidant, or hydrocarbon may have detrimental effects, both on the selectivity of oxidation and on foam stability [23,24].

This work is part of the MOUSTIC project which focuses on the development of innovative technologies for the *in situ* remediation of unsaturated soils contaminated by petroleum hydrocarbons. Previously, we reported an innovative surfactant foam-based technology to improve the control of reagent-delivery in model soils made of monodisperse glass beads [25]. Here, the performance of this new technology was compared with the traditional remedial fluids (water and surfactant solution) first, to distribute PS in 2D-sandboxes filled with real coal tar unsaturated and anisotropic soils having different grain sizes, permeabilities and contamination levels, and second, to remove hydrocarbons. Considering various permeability and wettability contrasts, this study allowed a better understanding of fluids' behaviors in anisotropic contaminated fields. PS-distributions in sandbox were accurately mapped and compared to visual observations. Comparison of hydrocarbons degradation rates and oxidation selectivity was carried out to assess any detrimental effect on the treatment efficiency. Only a few studies compared the use of water, surfactant solution and foam to deliver remedial reagents, namely nano zero-valent iron into porous media made of glass beads [21,26], or calcium polysulfide and phosphate into non-contaminated sediments [11,18]. A comparative study to deliver oxidizing agents using such fluids was never reported in real unsaturated soils contaminated with hydrocarbons in 2D-sandboxes. This represents a challenge regarding detrimental interactions between surfactant and oxidant [24,25]. This work aims to demonstrate the interest of the foam-based method in situations often observed in polluted sites.

2. Materials and methods

2.1. Chemicals

Zwitterionic surfactant Lauryl betaine (LB) was used either directly for S-PS or to generate foams for F-PS [24,25]. The contaminant was a liquid coal tar (density 1.15) collected from a former steelwork industrial site, whose composition is provided in Table SM.1. Briefly, the measured fraction of hydrocarbons in coal tar were 56.4 and 42.3%w for C5-C9 (volatile) and C10-C40 (semi-volatile), respectively. Sodium persulfate (>96%, Fisher Scientific) was used as oxidant, because of its higher selectivity towards aromatic hydrocarbons when surfactant is present [24]. Analytical reagents were dichloromethane (>99%, Fisher), n-hexane (99%, VWR), iodide and potassium iodide (99.9%, Fisher), barium chloride dihydrate (>99%, VWR), elementary iron (Prolabo). All solutions were prepared with deionized water.

2.2. Soils

Two mostly quartzic soils with low carbonate content were used in this study: a silty (ST) and a sandy soil (SD), both locally sourced. The raw sandy soil was sieved under running water to collect a fine (FSD) and coarse fraction (CSD). These two soils were then artificially contaminated by coal tar according to [25]. Four levels of tar contamination were prepared (0.2, 1, 5 and 10 $g.kg_{soil}^{-1}$) and the soils were aged for five months in sealed glass flasks stored upside-down to avoid hydrocarbon volatilization. The soils' surface areas were estimated by calculation using the particle size distribution, assuming spherical particles. Pore radii were estimated to be equal to $D_{10}/2$ (10^{th} percentile of grain size distribution) for each material assuming that, permeability is mostly affected by smaller grains [27]. Main characteristics of the soils used in this study are summarized in Table SM.2.

2.3. Experimental set-up

The experimental set-up used for fluids injection experiments is presented in Figure 1.

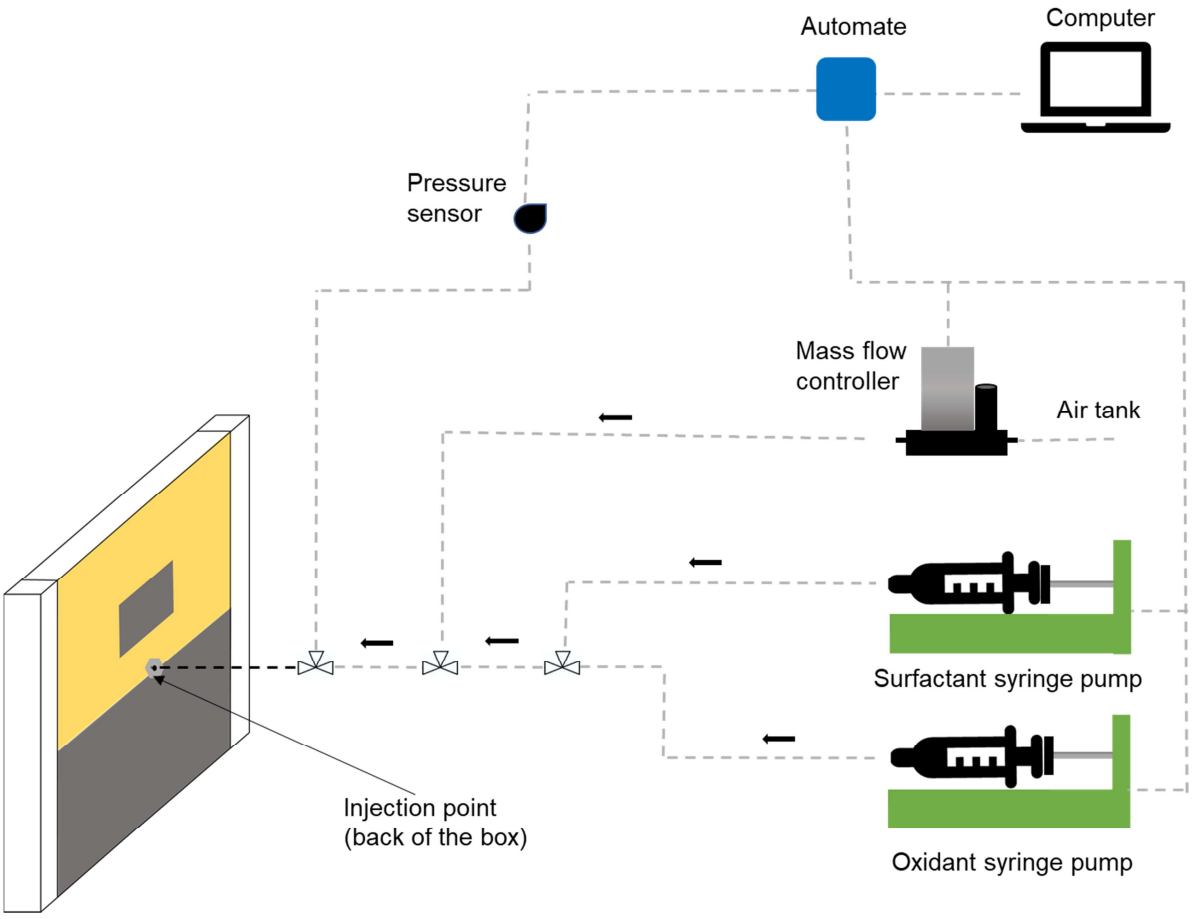

101 Figure 1. Scheme of the experimental set-up for fluids injection in packed sandbox.

102 Soils were packed in a PMMA 2D-sandbox (internal dimensions: 25 cm wide, 2 cm thick, 18 cm high).
103 The front face was removable thanks to screws and gasket. Soil was compacted using a rubber stick
104 while filling. Top lid and gasket were then tightly held using clamps to ensure perfect sealing. All
105 experiments were conducted under unsaturated conditions.

106 Four anisotropic models were studied: two contamination contrasts, where soil permeability was set
107 at 90 µm² and two permeability contrasts with tar-contamination set to 5 $g.kg^{-1}$. As shown in Fig. 1,
108 the materials were set as two horizontal layers (9 cm high). A rectangular lens (6 cm wide x 3 cm
109 high) of the bottom layer material was embedded within the upper layer. The selected configurations
110 are summarized in Table 1.

111 Table 1: Summary of the sandbox experiments for persulfate delivery.

Contrast	Upper layer soil	Bottom layer soil	Embedded lens soil
C1: contamination 1st case: clean and moderately contaminated soil	FSD0 90 µm^2 0 g.kg^{-1}	FSD5 90 µm^2 5 g.kg^{-1}	FSD5 90 µm^2 5 g.kg^{-1}
C2: contamination 2nd case: contrast of 1:10	FSD1 90 µm^2 1 g.kg^{-1}	FSD10 90 µm^2 10 g.kg^{-1}	FSD10 90 µm^2 10 g.kg^{-1}
P1: permeability 1st case: contrast of 1:18	FSD5 90 µm^2 5 g.kg^{-1}	CSD5 1362 µm^2 5 g.kg^{-1}	CSD5 1362 µm^2 5 g.kg^{-1}
P2: permeability 2nd case: contrast of 1:23	FSD5 90 µm^2 5 g.kg^{-1}	ST5 4 µm^2 5 g.kg^{-1}	ST5 4 µm^2 5 g.kg^{-1}

112 All fluids were injected at the center of the sandbox by an opening at the back (i.d. 0.8 mm, Fig. 1).
113 Syringe pumps, flow-meter and pressure sensor were as in [25].

114 2.4. Injection procedures

115 2.4.1. Foam injection

116 Prior to PS-injection, foam was formed into the soil [25]. For C1, C2 and P2, foam was injected using
117 the solution alternating gas (SAG) method, since it requires the lowest pressure for injection in soils
118 with such permeability [15,28]. Slugs of air and surfactant (1%w) were injected in alternation. Flow
119 rates and volumes per cycle were 70 and 2 mL.min^{-1} and 5 and 0.2 mL for gas and surfactant,
120 respectively. For P1 experiment, due to the presence of the highly permeable CSD5, foam was pre-

generated by co-injecting surfactant and gas through a pre-column (9 cm) filled with FSD0. For pre-generated foam, flow rates were 700 $mL.min^{-1}$ and 8 $mL.min^{-1}$ for gas and surfactant solution, respectively (foam quality (FQ) = 99%). A pressure limit at 100 $kPa.m^{-1}$ was set for injection in each experiment to avoid soil fracturing or heaving [29].

2.4.2 Persulfate injection

Non-activated PS (10 $g.L^{-1}$) was delivered in three forms with increasing complexity: solubilized in water (W-PS), in LB (1%w) surfactant solution (S-PS), or as solution in water delivered after foam injection (F-PS). The injected PS-concentration was chosen mainly to limit dilutions for soil analyses used to map PS-delivery. This was acceptable, since PS-concentration does not affect foamability of the surfactant even at high concentrations close to its solubility limit [24].

For each situation, the volume of PS solution injected was the same for the three delivery fluids to allow comparison. The injected volume of PS solution was the volume that filled the foam occupied area and moved surfactant from the network of lamellae. It was estimated according to F-PS experiments [25]. This was achieved by calculating the porous volume of soil occupied by foam using the ImageJ software [30]. Injected volumes of PS solution were 80, 120, 90 and 50 mL for C1, C2, P1 and P2, respectively.

2.5. PS-analysis in sandboxes

2.5.1. PS-distribution in contaminated anisotropic sandboxes

For all injection experiments, with the three fluids in the four configurations (C1, C2, P1, P2), pictures of the sandbox were taken periodically (see Fig. SM.1 and SM.2). However, evaluating the oxidant distribution only visually may be inaccurate. To overcome this limitation, PS-concentrations were locally measured across the sandbox. Soil was thoroughly sampled after the removal of the sandbox's front face. Mapping of PS-concentrations ($g.kg_{soil}^{-1}$) was done for every experiment after PS-injection according to [31,32]. Details can be found in the supplementary material.

To quantify PS-distribution efficiency, an isotropic distribution factor, (I_f, dimensionless) was calculated according to Eq.1. The I_f is the PS concentration-weighted ratio of its propagation distances in the vertical and horizontal directions from the injection point, which allows the comparison of delivery and sweeping efficiency between experiments.

$$I_f = \frac{\sum dv^- Cv^- / \sum dv^+ Cv^+}{\sum |dh| Ch / \sum |dv| Cv} \quad (1)$$

where d and C are the propagation distance and the PS-concentration at a given distance from the injection point, respectively. The indexes v and h represent the vertical and horizontal directions, respectively and the + or – signs indicate the upper and lower or right and left direction for the vertical and horizontal distances, respectively. Herein, the optimal value for I_f would be 1, representing an isotropic reagents distribution and meaning that the horizontal and vertical distribution of PS are equal. In contrast, high or low I_f-values indicate an anisotropic distribution of reagents around the injection point.

The capillary number (N_c, dimensionless) is defined as the ratio of viscous forces to capillary forces. It is defined by Eq.2 and was calculated for each PS-delivery fluid [33].

$$N_c = \frac{\mu u}{\gamma} \quad (2)$$

where μ is the injected fluid apparent viscosity (Pa.s), $u$is the fluid velocity (m.s^{-1}), and γ is the interfacial tension (IFT) at the air/solution interface (N.m^{-1}). It allows a quantitative assessment of forces controlling the remedial fluid propagation. Here, flow rates for W-PS, S-PS and surfactant solution when injecting foam were unchanged (Q= 2 mL.min^{-1}). The effective viscosity of the foam was estimated for C1 and C2 experiments from the Darcy Law:

$$\eta_{foam} = \frac{k.A}{Q}.\nabla P \quad (3)$$

where A is the cross-section used by foam to propagate, ∇P is the pressure gradient, and k is the soil permeability (m.s^{-1}).

2.6. Contact angles and interfacial tension measurements

The contact angle θ at which an air–water interface meets a solid surface [34] (Fig. SM.1), is an important measurement directly linked to surface wettability. It controls the rate and amount of spontaneous imbibition of water by soil [35]. It can be calculated using the Young equation [36]:

$$\cos\theta = \frac{\gamma_{nw-s} - \gamma_{w-s}}{\gamma_{nw-w}} \quad (4)$$

where w, nw and s are the liquid wetting and non-wetting phases, and the solid phase, respectively. Solid phases in this study were the different soils presented in Table SM.2. The wetting and non-wetting phases were air and/or water-based solutions depending on the experimental conditions (see §2.7 for details). θ-values less than 90° indicates a water-wet solid phase, or an oil-wet solid if higher; The latter impeding the spontaneous infiltration of the aqueous phase into the porous medium.

θ were measured using the modified sessile drop method for all soils using PS-solution in water or aqueous surfactant [37].

The IFT at the air/solution interface was measured for PS solution in water or surfactant, using the pendant drop method [14].

2.7. Liquids entry pressure calculations

Capillary forces play an important role in fluids circulation in porous media [38]. The entry capillary pressure in pores P_{ce} (Pa), is given by the Young–Laplace equation [39]:

$$P_{ce} = \frac{2\gamma}{R}\cos\theta_w \quad (5)$$

where θ_w is the contact angle of the wetting phase and R is the pore radius (m).

The non-wetting phase flows into the porous medium when the capillary pressure ($P_c = P_{nw} - P_w$) exceeds P_{ce}.

For $\theta < 90°$, the wetting phase is the liquid, the non-wetting phase is the air and $\theta_w = \theta_{liquid}$. Air replacement by water occurs when P_c remains lower than P_{ce}.

$$P_c < P_{ce} P_{nw} - P_w < P_{ce}$$

$$P_{air} - P_{liquid} < \frac{2\gamma}{R}\cos\theta \leftrightarrow P_{liquid} - P_{air} > \frac{-2\gamma}{R}\cos\theta \quad (6)$$

which gives the excess of pressure that should be applied to liquid (compared to air) in order it propagates into the soil.

For $\theta > 90°$, the wetting phase is the air and the non-wetting phase is the liquid, so $\theta_w = \theta_{air} = 180 - \theta_{liquid}$ and then $\cos\theta_{liquid} = -cos\theta_{air}$ which explains the change of sign in the right side of Eq.6.

2.8. Hydrocarbons degradation experiments

To compare the oxidation efficiency of hydrocarbons by PS delivered with the three methods, the fine sandy soil (FSD0) was contaminated at 200 ± 14 mg.kg_{soil}^{-1} (FSD02). The latter was hydrophilic and water-wet. This lower contamination level was chosen to not penalize the efficiency of traditional water-based delivery methods and to avoid high oxidant doses in the media. W-PS and S-PS experiments were performed in stirred glass batch reactors to ensure good contact between contaminated soil and PS. In these experiments, 101 mL of oxidant solution was mixed with 290 g of contaminated soil. F-PS experiments were carried out, in vertical glass columns (length: 18 cm high, i.d.:3.6 cm). In those experiments, foam was injected first, then PS-solution. PS was injected until all surfactant solution was pushed away from the foam zone. This PS-volume was estimated to be about 30.4 mL, considering that water saturation after foam injection is 30%. Injection flow rates were the same as in § 2.4. Two PS doses were assessed and calculated from the stoichiometric molar ratio (SMR) between PS and benzene. The latter was assumed as a model organic compound to represent the entire coal-tar mass, as previously reported [40]. Those doses corresponded to 1 and 3 SMR and were equal to 9.1 and 27.4 $g_{PS}.kg_{soil}^{-1}$, respectively. In all cases, after PS was injected, the

contaminated soil was quickly transferred in glass bottles and placed at 60°C in a thermostated water bath for PS-activation. Four control experiments without oxidant, using the 3 compared methods were also carried out. After 70h-contact, total petroleum hydrocarbon (TPH) indexes measurements for semi-volatile fractions were obtained according to the NF EN ISO 9377-2 method, after 25 g of soil were extracted three-times at room temperature using n-hexane.

2.9. Selectivity calculation

The selectivity of hydrocarbons degradation illustrates the preferential degradation of hydrocarbons over the surfactant. It was calculated as follows:

$$Selectivity = \frac{k_{obs,hydrocabons}}{k_{obs,Surfactant}} \quad (7)$$

Where $k_{obs,hydrocabons}$ and $k_{obs,Surfactant}$ are the pseudo first-order oxidation rate constants for hydrocarbons and surfactant, respectively, obtained by linear fitting of concentrations *vs.* time.

3. Results and discussions

3.1. Contact angle evolution with contamination, permeability and surfactant presence

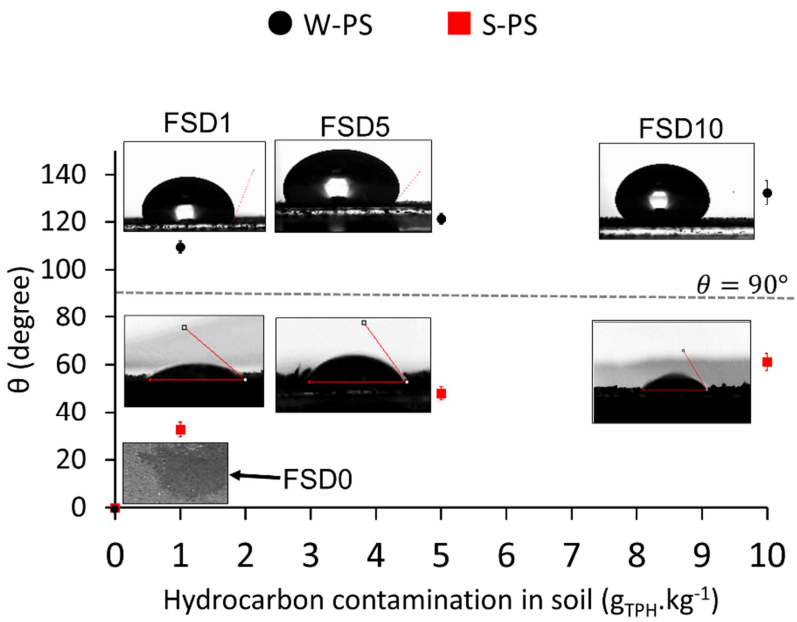

A

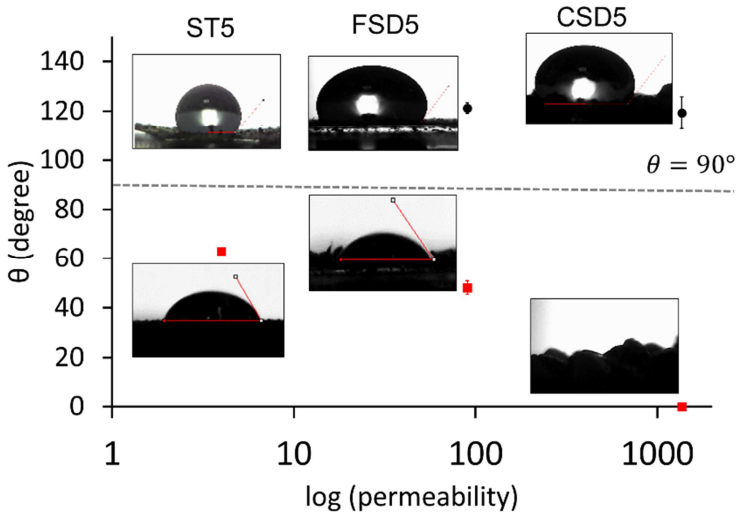

B

Figure 2. Contact angles (θ) measured for the soils used in this study: a) 90 µm² permeability FSD soils with different hydrocarbon contamination levels (FSD0 – FSD10) and b) 5 $g_{TPH}.kg^{-1}$ contaminated soils with different permeabilities (ST5 – CSD5). PS in water (W-PS, ●) and in 1% surfactant solution (S-PS, ■).

Contact angles measured for PS in water and surfactant solution with the soils are presented in Fig. 2. The non-contaminated sand was totally water-wet (θ = 0°). For all the contaminated materials, in absence of surfactant, θ were above 90° because of their hydrophobicity. For the 90 µm² contaminated soil, θ, and, as a result, the hydrophobicity of the soil, increased from 115 to 130° for hydrocarbon concentrations ranging from 1 to 10 $g.kg^{-1}$ (Fig. 2a), showing that higher contaminated soils are more hydrophobic.

As shown in Fig. 2, the presence of surfactant decreased θ below 90° for all contaminated soils, showing the alteration of wettability from oil-wet to water-wet [41]. However, θ still increased from 35 to 61° for hydrocarbon concentrations ranging from 1 to 10 $g.kg^{-1}$, respectively, because of the higher soil hydrophobicity.

3.2. Contamination-contrasted sandboxes

Concentration maps for PS delivery using the three compared methods of injection are plotted in Figure 3 for the contrast contamination models C1 and C2.

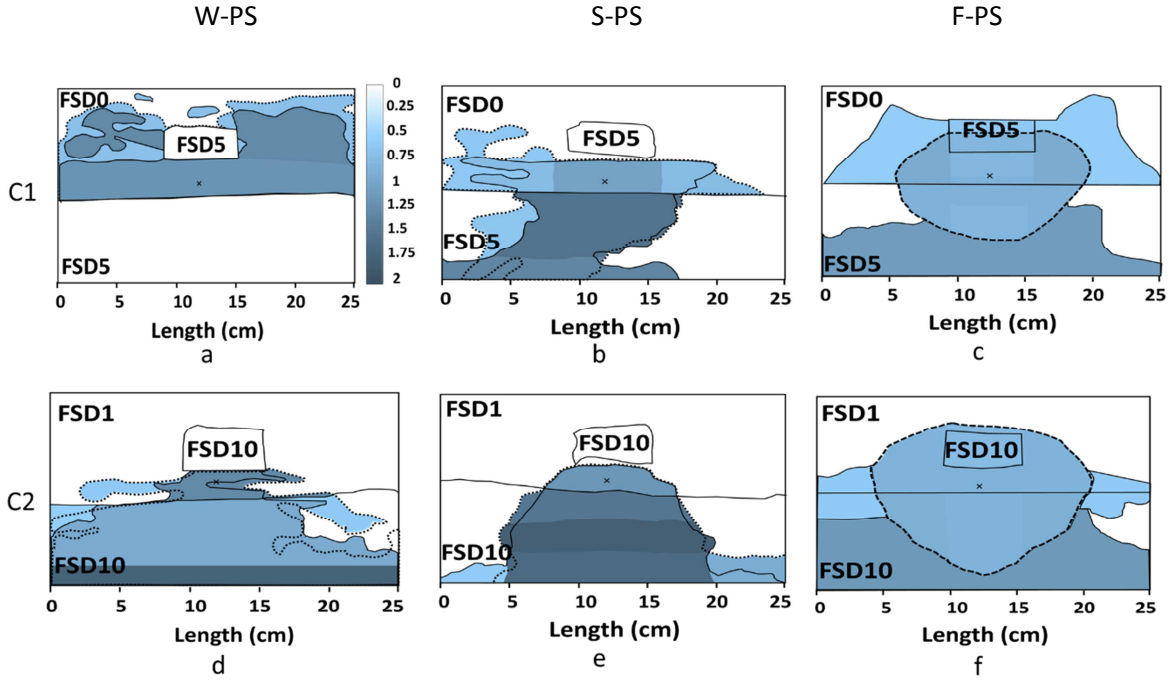

Figure 3. PS-concentration maps ($g.kg_{soil}^{-1}$) in contamination contrasted sandboxes. Black cross indicates the injection point. Solid, and dotted lines represent the wet areas at front and back sides, respectively. For F-PS experiments, dashed lines represent the foam limit. PS-concentrations varied from 0 (white) to 2 $g_{PS}.kg_{soil}^{-1}$ (dark blue).

Considering C1, when W-PS was used as a delivery fluid, it propagated only in the non-contaminated area (Fig. 3a). No entrance into the contaminated zones was observed. Two mechanisms occurred: on the one hand, in the clean zone, the soil was strongly water-wet and capillary suction attracted water within the pore spaces. Comparing the evolution of $P_{liquid} - P_{air}$ using W-PS and S-PS in the studied soils (Fig. 4), the negative value of $P_{liquid} - P_{air}$confirms capillary suction. On the other hand, the hindered water flow into the contaminated soil was emphasized because of its strong hydrophobicity (Fig. 2a) and the higher capillary pressure required for the liquid to flow into it. For C2 using W-PS, a different behavior was observed, since the strong hydrophobicity of soils caused an important edge effect and water did not propagate into the soil. Indeed, when using water, the edge effect altered the visual observations that were no longer representative of actual PS-concentrations. Water propagated preferentially along the cell walls which were more water-wet than the soil. Fig. SM.2 compares the visual propagation of PS and its actual concentrations (see Figs. SM.3 and SM.4 for the rest of the experiments). Visually, it seems that water propagated in the whole contaminated bottom layer uniformly, saturating it. However, this visual observation was inaccurate since measured PS-concentration in this area was low (Fig. SM.2b). Thus, experimenters should beware of edge effects, especially occurring for solutions with high interfacial tensions, that might not be always representative of reality. In this case, calculated $P_{liquid} - P_{air}$ were high for both soils and increased about 2-times with contamination for FSD1 and FSD10, respectively (Fig. 4a). It explains the difficulty for water to flow into hydrophobic zones and its inefficiency to deliver PS. PS-distribution within the swept area was heterogeneous, and its concentration varied 2.3 and 6.8-times between lowest and highest PS-concentrations for C1 and C2, respectively. This could be explained by local soil heterogeneity, affecting water saturation. For water-delivered PS in C1 and C2, the I_f- value obtained

from visual observations is wrong, since the water propagated only within the clean layer (C1) and only along the cell walls (C2).

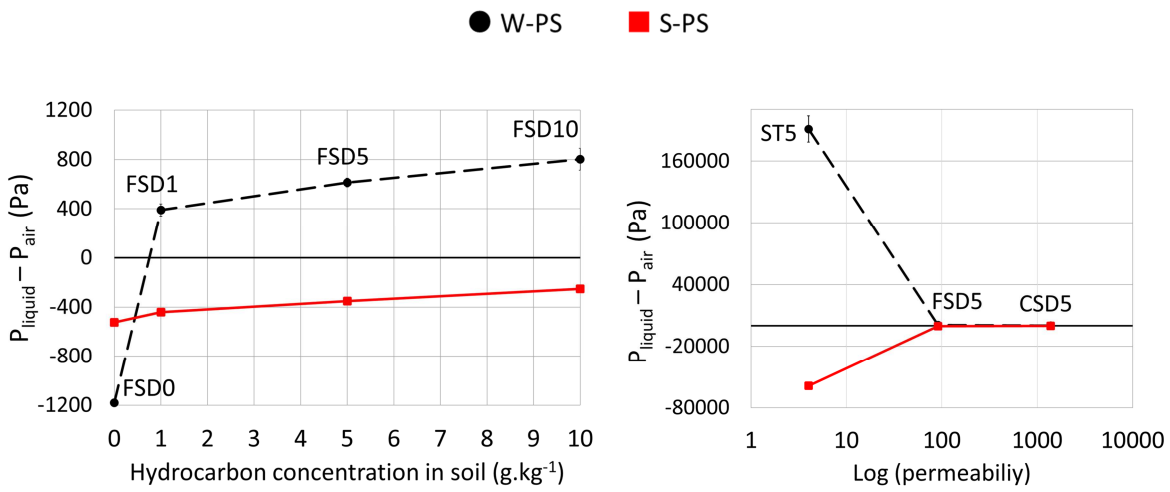

a b

Figure 4. Evolution of $P_{liquid} - P_{air}$ with hydrocarbon concentration for W-PS (●) and S-PS (■) calculated from eq. 6: a) 90 µm² permeability FSD soils with different contaminations levels (FSD0 – FSD 10) and b) 5 g.kg^{-1} contaminated soils with different permeabilities (ST5 – CSD5).

When surfactant was added (S-PS), PS-distribution was enhanced, compared to W-PS, both for C1 and C2 (Figs 3b and 3e), thanks to two mechanisms: first, the reduction in the air–water IFT from 72 to 32 mN.m^{-1}, which yielded a slight increase in N_c from 3.68 to 8.28×10^{-5} for W-PS and S-PS, respectively (Table SM.3); The effect of capillary forces was reduced twice. Second, surfactant adsorption reversed soil wettability, from oil-wet to water-wet (Fig. 2) [41,42]. This change to water-wet behavior promoted the spontaneous imbibition of the contaminated zone, as confirmed by negative $P_{liquid} - P_{air}$ values in Fig.4a. Hence, surfactants proved to be beneficial for enhancing PS-delivery in hydrocarbon-wet contaminated soils, as previously reported [20]. However, within the wet zone, as observed for W-PS, PS-concentrations remained heterogeneous and varied 2.8 and 3.6-times for C1 and C2, respectively. As reported in Fig. 5 which summarizes I_f-values, the latter was quite high and equal to 4.57 and 12.74 for S-PS in C1 and C2, respectively. Despite a great enhancement compared to W-PS, the PS-distribution was still anisotropic, and its vertical distribution

was more important than its horizontal one. Besides, both for W-PS and S-PS, the contaminated lens embedded in the upper layer was not swept by the oxidant.

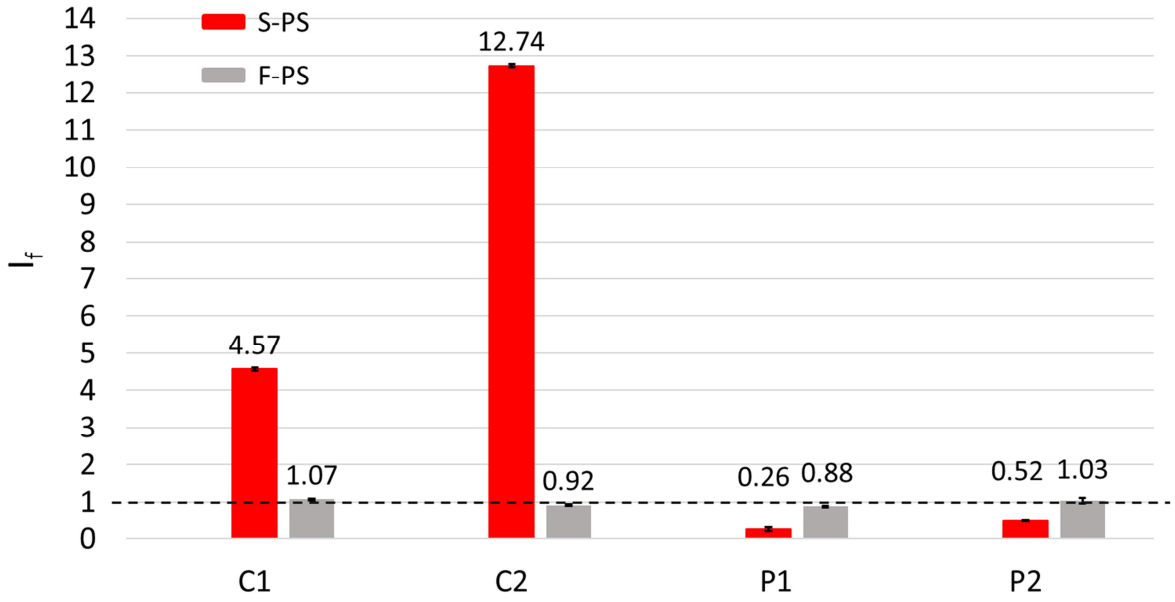

Figure 5. Isotropic delivery factor (I_f) values for contamination contrasts (C1 and C2) and permeability contrasts (P1 and P2) experiments, using S-PS and F-PS delivery methods. Horizontal dashed line at I_f = 1 represents an ideally isotropic PS-distribution. Error bars are shown for each experiment.

Contamination contrasted media only slightly affected the propagation of foam, which flowed in every direction around the injection point without any viscous fingering (Fig. 3c,f), as previously reported [11,12,21,25,43]. In contrast to solutions, foam propagation was mainly controlled by its high viscosity (168. 10^{-3} Pa.s) and its shear-thinning behavior, that overcame gravitational effects and fingering [44]. As for S-PS, the use of foam decreased the air–water IFT from 72 to 32 $mN.m^{-1}$. In order to maximize the selectivity of the oxidation, PS was injected only once foam was set in place, as previously described [25]. PS-delivery around the injection point was much more isotropic when the F-PS method was used. The PS solution efficiently swept the contaminated lens situated above the injection point. Horizontal and vertical PS-distributions were roughly equal as demonstrated by the I_f-values amounting to 1.07 and 0.92 for C1 and C2, respectively (Fig. 5). In the meantime, N_c,

increased at least by 150-times from S-PS to F-PS, as shown in Table SM.3, improving the sweeping efficiency of the foam in contamination contrasted media [45]. Surfactant drainage was observed due to the unsaturated conditions and destabilizing effect of hydrocarbons on foam lamellae, as explained previously [25]. In addition, the PS-concentration was very homogeneous within the foam network and varied less than 1.3-times for C1 and C2 (Fig. 3c). The maximal PS-concentration that can be delivered was 1.03 $g_{PS}.kg_{soil}^{-1}$, considering both the injected PS solution (10 $g.l^{-1}$) and a typical water saturation of 30% within the foam network. To deliver higher PS-concentrations in soil using foam, larger PS-concentrations in solution have to be used, with the aim of overcoming the lower water saturation when using the foam-based method. PS-concentrations in soil were higher in the liquid drainage zone outside the foam than inside, because of the higher water saturation. Nevertheless, the injection of an excessive volume of PS may be avoided by better evaluating the volume of liquid to replace in the foam zone. PS remains trapped in place for months despite foam decay with time, because water is trapped by capillary forces.

3.3. Permeability-contrasted contaminated soils

Considering strong permeability contrasts in contaminated soils, two situations were studied. In the former (P1), the medium was built using a high and a moderate permeability soil, whereas in the latter (P2), moderate and low permeability soils were used. PS-concentration maps using the compared methods of oxidant delivery are plotted in Figure 6.

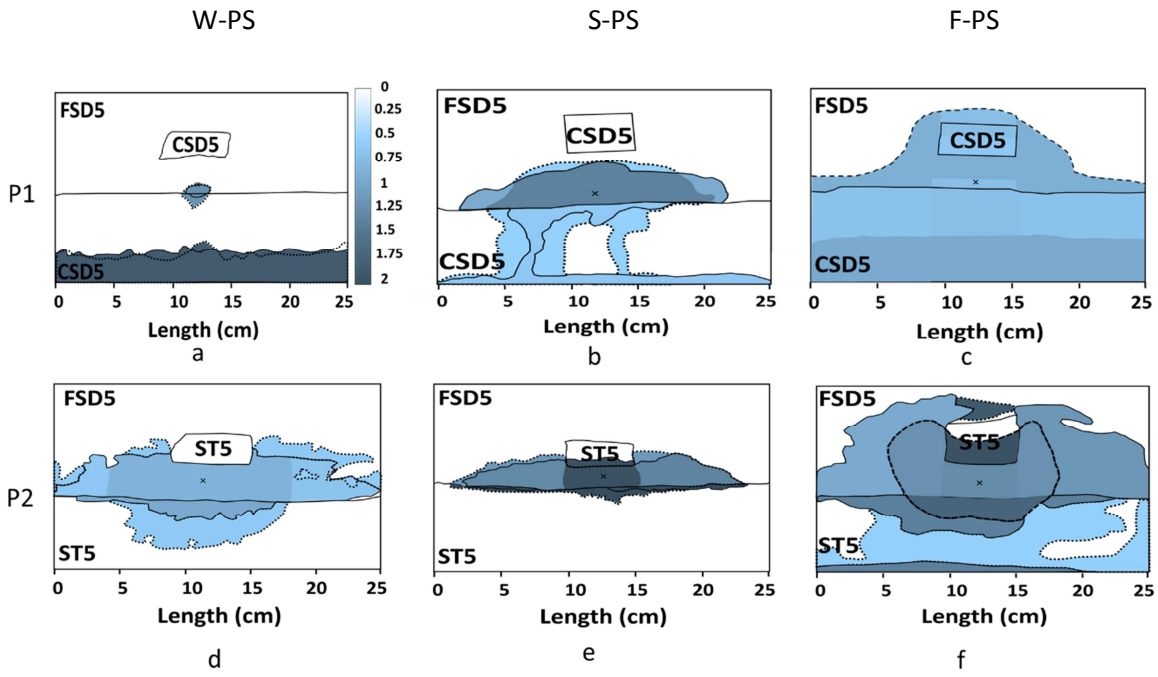

Figure 6. PS-concentration maps (g.kg$_{soil}^{-1}$) for permeability-contrasted sandboxes using the three delivery methods. Black cross indicates the injection point. Solid, and dotted lines represent the wet areas at the front and back sides, respectively. For F-PS experiments, dashed lines represent the foam limit. PS-concentrations varied from 0 (white) to 2 g.kg$_{soil}^{-1}$ (dark blue).

3.3.1. Permeability contrast in a moderate to high permeability medium (P1)

For P1, using the W-PS method of injection, the solution accumulated in the most permeable bottom layer where PS-concentration was maximal (Fig. 6a). Downward water flow resulted from the low capillary retention caused by the large pore throats of the soil and the transport was only controlled by gravity. Since no horizontal PS-distribution was observed, the I_f-value was set to zero. Despite smaller pore size, the upper layer was avoided because its high hydrophobicity and higher $P_{liquid} - P_{air}$. Besides, important edge effects were observed when using W-PS in P2, like for C2, due to the hydrophobicity of the soils and the low permeability of ST5. In this case, $P_{liquid} - P_{air}$ were 613 and 1.9×10^6 Pa for FSD5 and ST5, respectively (Fig. 4b). The huge contrast of $P_{liquid} - P_{air}$ values between FSD5 and ST5 led to the complete avoidance of ST5 layer by water and to 2.8-times variability in PS-concentration between the zones.

The addition of surfactant had similar effects as presented in §3.2, causing the inversion of soils wettability for P1 (Fig. 2) and the elimination of the edge effect for P2, as confirmed by the PS-concentration map (Fig. 6e). For P1, the value of $P_{liquid} - P_{air}$ dropped significantly when the surfactant was used for both contamination levels (5 and 10 g.kg^{-1}, Fig. 4b). This led to a higher suction of the solution in both layers and a better horizontal oxidant distribution compared to water alone (Fig. 6b). However, in the CSD5 layer, gravity forces still had strong effects and altered the migration of the surfactant solution, since preferential pathways were observed in the bottom layer. Conversely, in the case of P2, the solution only propagated 2 cm vertically in ST5 and spread horizontally into the most permeable layer (FSD5). In fact, adding surfactant did not seem to inverse wettability of the low permeability soil as expected from θ-values (Fig. 2b). Indeed, $P_{liquid} - P_{air}$ value should have, theoretically, decreased from 3207 to -5.9×10^4 Pa and the solution should have been sucked preferentially in this zone. However, the oxidant only accumulated in the most permeable upper layer. In fact, the surface area of the silt, which was 3-times higher than the sand, caused a bigger surfactant adsorption [46,47]. Hence, the wettability inversion was probably slower in this zone, compared to the high permeability layer. For permeability contrast experiments using S-PS, the I_f-values were very low (Fig. 5) and PS-concentrations remained very heterogeneous since they varied more than 5-times. Using a direct injection of PS solutions, the contaminated lens above the injection point was never swept, following the example of C1 and C2.

When using the F-PS method, the PS-solution propagated within all the contaminated zones, regardless of the permeability contrasts, especially for P1 (Fig. 6c). In both cases, a slight effect of the permeability contrast on the foam propagation rate was noticed, since it propagated faster into the high permeability soil [28,46,47]. For P2, the foam propagation in the low permeability zone was slowed down by a higher destabilization rate caused both by the higher surface area and the hydraulic resistance of the material. Drainage was observed in both layers, like for C1 and C2.

Once the PS solution was injected, it distributed in the area occupied by foam and beyond. For P1, the PS-concentration was quite homogeneous inside the foam zone and varied only 1.6-times. For P2, in contrast to previous observations with foam, the PS-distribution was not so homogeneous inside the foam network; a variability of 2.9-times was observed in PS-concentrations (Fig. 8f). However, it is still satisfying, since PS successfully distributed into the ST5 zone too. In this zone, the PS-concentration was 2 $g.kg_{soil}^{-1}$. It is beyond the maximal value expected within the foam, and it shows the destabilization of the latter, since such concentrations can only be obtained when the solution saturates the pores. Moreover, the F-PS method successfully delivered the oxidant into the low permeability zones. For both permeability contrast experiments using F-PS, the I_f-values were closer to one, despite the complex behavior of foam and the PS-distribution in P2 (Fig. 5). This observation confirmed that, the PS-distribution was rather homogeneous in the case of the whole sandbox, for P2.

3.4. Comparative oxidation of hydrocarbons

Considering the removal of hydrocarbons in comparative degradation experiments, controls were performed in order to better amount what is related to oxidation. Hydrocarbons removal rates in control experiments increased in the following order: foam (0.11 ± 0.03%) < surfactant (2.70 ± 2.02 %) < water (5.50 ± 2.00 %). Naphthalene and phenanthrene were identified as major components of the removed fraction, and the volatilization was assumed to be the main phenomenon for non-specific removal. Thus, the previous order is explained by the micelles stabilizing effects towards hydrocarbons and by the bubbles, which hindered the volatilization of the contaminant by trapping it into the soil.

After 70 h of contact with the oxidant, hydrocarbons removal rates were very high for all of the PS-concentrations and methods, showing that the SMR estimation was correct. Hydrocarbons removal rates followed the order W-PS > F-PS > S-PS. Increasing PS-concentration slightly increased

hydrocarbons removal rates, because it promoted the generation of more free radicals in solution (*i.e.* $S_2O_8^{2}$, $SO_4^{\bullet-}$ and $HO^{\bullet}$) as reported [24,48–51]. For 1 and 3-SMR, hydrocarbon removal rates were: 95.6 (0.5)% and 99.2 (0.8)% for W-PS; 92.2 (1.2)% and 97.0 (1.3)% for S-PS; and 95.0 (1.1)% and 98.6 (1.8)% for F-PS, respectively.

The contaminated soil used here was initially water-wet and mixed before activation in W-PS and S-PS experiments; Therefore the contact between PS and contamination was optimal, leading to high oxidation efficiencies even for W-PS. However, with hydrophobic soils ($coal\ tar \geq 1$ g.kg_{soil}^{-1}), as seen in §3.1 and 3.2, the conditions would not be so favorable [25,26] and the oxidation using the W-PS method is expected to be low. The slightly higher degradation of hydrocarbons using F-PS compared to S-PS was explained by the lower content of surfactant in the soil after the PS-injection, since the latter pushed away about 80% of the initial surfactant used to generate foam. Considering the calculated selectivity of hydrocarbons oxidation, the increasing of the PS-concentration had no significant effect (0.33 ± 0.02 and 12.31 ± 0.19) for S-PS and F-PS methods, respectively, in agreement with previous report [13]. However, the sequential delivery of PS using the F-PS method improved the selectivity of the oxidation by 38-times, as expected, since it removed the 80% of the surfactant from the soil pores. Thus, non-productive oxidant consumption by surfactant was lowered when using the F-PS method. Consequently, even though hydrocarbons degradation rates were similar between F-PS and W-PS methods in the tested conditions, gains are expected to be higher when injections occur in more hydrophobic media (Figs 3 and 6). The most important aspect is that despite the adverse comparative conditions used in this study, the foam-based method did not show any detrimental effect regarding the oxidation of hydrocarbons. Even more, it showed a better degradation efficiency and a more uniform oxidant distribution than usual S-ISCO, carried out using full mixing of soil and oxidizing solutions.

4. Conclusion

Three PS-delivery methods, with increasing complexity, were compared to distribute PS in unsaturated coal tar-contaminated soils with high permeability or contamination contrasts. Pure water proved to be the less favorable method to deliver PS in such contaminated soils, since the hydrophobicity of the latter had a strong impact on oxidant-distribution. The addition of surfactant lowered IFT and inverted the wettability of the contaminated materials. It resulted in enhanced PS propagation into the contaminated zones. However, gravity forces still led to preferential circulation pathways. The most isotropic PS-distributions were obtained when this oxidant was delivered within a foam network, which is much more viscous than traditional fluids. The oxidizing solution exhibited the best sweeping efficiency when it was delivered using the foam-based method and its propagation was only slightly affected by gravity. Moreover, despite unfavorable comparative conditions to the usual methods, the sequential injection of foam and PS solution did not show any detrimental effect regarding the removal of hydrocarbons. The latter was very high for the tested PS-concentrations. The foam-based method proved to be more selective than the usual S-ISCO, due to the lower surfactant content in the oxidized zone. To deliver higher PS-concentrations in soil using the foam-based method, larger PS-concentrations of the injected solution have to be used, in order to overcome the lower water saturation in the soil, by using this foam-based method.

5. Acknowledgements

This research was carried out as a part of the MOUSTIC project funded by the French National Research Agency (ANR-15-CE04-0011).

6. References

[1] P.S. Birak, C.T. Miller, Dense non-aqueous phase liquids at former manufactured gas plants : Challenges to modeling and remediation, J. Contam. Hydrol. 105 (2009) 81–98. doi:10.1016/j.jconhyd.2008.12.001.

[2] S.C. Hauswirth, C.T. Miller, A comparison of physicochemical methods for the remediation of porous medium systems contaminated with tar, J. Contam. Hydrol. 167 (2014) 44–60. doi:10.1016/j.jconhyd.2014.08.002.

[3] US EPA, In Situ Treatment Technologies for Contaminated Soil, 2006.

[4] B. Ranc, P. Faure, V. Croze, M.O. Simonnot, Selection of oxidant doses for in situ chemical oxidation of soils contaminated by polycyclic aromatic hydrocarbons (PAHs): A review, J. Hazard. Mater. 312 (2016) 280–297. doi:10.1016/j.jhazmat.2016.03.068.

[5] F.J. Rivas, Polycyclic aromatic hydrocarbons sorbed on soils: A short review of chemical oxidation based treatments, J. Hazard. Mater. 138 (2006) 234–251. doi:10.1016/j.jhazmat.2006.07.048.

[6] P.J. Dugan, R.L. Siegrist, M.L. Crimi, Coupling surfactants/cosolvents with oxidants for enhanced DNAPL removal: A review, Remediat. J. 20 (2010) 27–49. doi:10.1002/rem.20249.

[7] W.H. Wang, G.E. Hoag, J.B. Collins, R. Naidu, Evaluation of surfactant-enhanced in situ chemical oxidation (S-ISCO) in contaminated soil, Water. Air. Soil Pollut. 224 (2013) 1–9. doi:10.1007/s11270-013-1713-z.

[8] G. Dahal, J. Holcomb, D. Socci, Surfactant-Oxidation Co-Application for soil and gruondwater remediation, Remediat. J. 26 (2016) 101–108. doi:10.1002/rem.20290.

[9] M. Abtahi, A Novel Combination of Surfactant Addition and Persulfate-assisted Electrokinetic Oxidation for Remediation of Pyrene-Contaminated Soil, Chem. Biochem. Eng. Q. 32 (2018) 55–69. doi:10.15255/CABEQ.2017.1204.

[10] F. Zheng, B. Gao, Y. Sun, X. Shi, H. Xu, J. Wu, Y. Gao, Removal of tetrachloroethylene from homogeneous and heterogeneous porous media: Combined effects of surfactant solubilization and oxidant degradation, Chem. Eng. J. 283 (2016) 595–603.

460 doi:10.1016/j.cej.2015.08.004.

461 [11] L. Zhong, J. Szecsody, M. Oostrom, M. Truex, X. Shen, X. Li, Enhanced remedial amendment
462 delivery to subsurface using shear thinning fluid and aqueous foam, J. Hazard. Mater. 191
463 (2011) 249–257. doi:10.1016/j.jhazmat.2011.04.074.

464 [12] Y.S. Zhao, Y. Su, J.R. Lian, H.F. Wang, L.L. Li, C.Y. Qin, Insights on flow behavior of foam in
465 unsaturated porous media during soil flushing, Water Environ. Res. 88 (2016) 2132–2141.
466 doi:10.2175/106143016X14733681695483.

467 [13] J. Maire, A. Joubert, D. Kaifas, T. Invernizzi, J. Marduel, S. Colombano, D. Cazaux, C. Marion, P.
468 Klein, A. Dumestre, N. Fatin-rouge, Assessment of flushing methods for the removal of heavy
469 chlorinated compounds DNAPL in an alluvial aquifer, Sci. Total Environ. 612 (2018) 1149–
470 1158. doi:10.1016/j.scitotenv.2017.08.309.

471 [14] J. Maire, N. Fatin-Rouge, Surfactant foam flushing for in situ removal of DNAPLs in shallow
472 soils, J. Hazard. Mater. 321 (2017) 247–255. doi:10.1016/j.jhazmat.2016.09.017.

473 [15] J. Maire, A. Coyer, N. Fatin-rouge, Surfactant foam technology for in situ removal of heavy
474 chlorinated, J. Hazard. Mater. 299 (2015) 630–638. doi:10.1016/j.jhazmat.2015.07.071.

475 [16] C. Portois, E. Essouayed, M.D. Annable, N. Guiserix, A. Joubert, O. Atteia, Field demonstration
476 of foam injection to con fi ne a chlorinated solvent source zone, J. Contam. Hydrol. 214 (2018)
477 16–23. doi:10.1016/j.jconhyd.2018.04.003.

478 [17] X. Shen, L. Zhao, Y. Ding, B. Liu, H. Zeng, L. Zhong, X. Li, Foam , a promising vehicle to deliver
479 nanoparticles for vadose zone remediation, J. Hazard. Mater. 186 (2011) 1773–1780.
480 doi:10.1016/j.jhazmat.2010.12.071.

481 [18] L. Zhong, J.E. Szecsody, F. Zhang, S. V. Mattigod, Foam Delivery of Amendments for Vadose
482 Zone Remediation: Propagation Performance in Unsaturated Sediments, Vadose Zo. J. 9

(2010) 757. doi:10.2136/vzj2010.0007.

[19] L. Zhong, N.P. Qafoku, J.E. Szecsody, P.E. Dresel, Z.F. Zhang, Foam Delivery of Calcium Polysulfide to Vadose Zone for Chromium-VI Immobilization: A Laboratory Evaluation, Vadoze Zo. J. 8 (2009) 976–985. doi:10.2136/vzj2008.0124.

[20] R. Bajagain, S. Lee, S. Jeong, Chemosphere Application of persulfate-oxidation foam spraying as a bioremediation pretreatment for diesel oil-contaminated soil, Chemosphere. 207 (2018) 565–572. doi:10.1016/j.chemosphere.2018.05.081.

[21] Y. Su, Y. Zhao, L. Li, C. Qin, Enhanced Delivery of Nanoscale Zero-Valent Iron in Porous Media by Sodium Dodecyl Sulfate Solution and Foam, Environ. Eng. Sci. 32 (2015) 684–693. doi:10.1089/ees.2014.0529.

[22] H. Wang, J. Chen, Enhanced flushing of polychlorinated biphenyls contaminated sands using surfactant foam: Effect of partition coefficient and sweep efficiency, J. Environ. Sci. (China). 24 (2012) 1270–1277. doi:10.1016/S1001-0742(11)60881-4.

[23] K. Osei-bonsu, N. Shokri, P. Grassia, Foam stability in the presence and absence of hydrocarbons: From bubble- to bulk-scale, Colloids Surfaces A Physicochem. Eng. Asp. 481 (2015) 514–526. doi:10.1016/j.colsurfa.2015.06.023.

[24] I. Bouzid, J. Maire, E. Brunol, S. Caradec, N. Fatin-Rouge, Compatibility of surfactants with activated-persulfate for the selective oxidation of PAH in groundwater remediation, J. Environ. Chem. Eng. 5 (2017) 6098–6106. doi:10.1016/j.jece.2017.11.038.

[25] I. Bouzid, J. Maire, S.I. Ahmed, N. Fatin-Rouge, Enhanced remedial reagents delivery in unsaturated anisotropic soils using surfactant foam, Chemosphere. 210 (2018). doi:10.1016/j.chemosphere.2018.07.081.

[26] L. Shi, J. Chen, Q. Wang, X. Song, Effects of carrier on the transport and DDT removal

performance of nano-zerovalent iron in packed sands, Chemosphere. 209 (2018) 489–495. doi:10.1016/j.chemosphere.2018.06.123.

[27] K. Terzaghi, R. B. Peck, Soil Mechanics in Engineering Practice, John Wiley and Sons, New York, 1964.

[28] J. Maire, E. Brunol, N. Fatin-Rouge, Shear-thinning fluids for gravity and anisotropy mitigation during soil remediation in the vadose zone, Chemosphere. 197 (2018) 661–669. doi:10.1016/j.chemosphere.2018.01.101.

[29] U. S. Environmental Protection Agency, Hydraulic Fracturing Technology:Technology Evaluation Report, 1993.

[30] C.A. Schneider, W.S. Rasband, K.W. Eliceiri, NIH Image to ImageJ : 25 years of image analysis, Nat. Methods. 9 (2012) 671–675. doi:10.1038/nmeth.2089.

[31] C.J. Cunningham, V. Pitschi, P. Anderson, D.A. Barry, C. Patterson, T.A. Peshkur, Field Application of a Rapid Spectrophotometric Method for Determination of Persulfate in Soil, PLoS One. 8 (2013) 6–11. doi:10.1371/journal.pone.0065106.

[32] J.W. Wimberley, The turbldimetric determination of sulfate without the use of additives, Anal. Chim. Acta. 42 (1968) 327–329. doi:10.1016/S0003-2670(01)80314-7.

[33] S.W. Jeong, Evaluation of the use of capillary numbers for quantifying the removal of DNAPL trapped in a porous medium by surfactant and surfactant foam floods, J. Colloid Interface Sci. 282 (2005) 182–187. doi:10.1016/j.jcis.2004.08.108.

[34] M.D. Murray, B.W. Darvell, A protocol for contact angle measurement, J. Phys. D. Appl. Phys. 23 (1990) 1150–1155. doi:10.1088/0022-3727/23/9/003.

[35] M. Amirpour, S.R. Shadizadeh, H. Esfandyari, S. Ahmadi, Experimental investigation of wettability alteration on residual oil saturation using nonionic surfactants: Capillary pressure

measurement, Petroleum. 1 (2015) 289–299. doi:10.1016/j.petlm.2015.11.003.

[36] L. Zhou, S. Das, B.R. Ellis, Effect of Surfactant Adsorption on the Wettability Alteration of Gas-Bearing Shales, Environ. Eng. Sci. 33 (2016) 766–778. doi:10.1089/ees.2016.0003.

[37] J. Bachmann, R. Horton, R.. Van Der Ploeg, S. Woche, Modified Sessile Drop Method for assessing initial soil-water contact angle of sandy soil, Soil. Sci. Soc. Am. J. 64 (2000) 546–567.

[38] D.B. Bennion, F.B. Thomas, R.F. Bietz, H. Energy, Low Permeability Gas Reservoirs : Problems, Opportunities and Solutions for Drilling , Completion, Stimulation and Production, in: SPE 35577, Society of Petroleum Engineers, Calgary, Alberta, Canada, 1996. doi:10.2118/35577-MS.

[39] V. Joekar-Niasar, S.M. Hassanizadeh, A. Leijnse, Insights into the relationships among capillary pressure, saturation, interfacial area and relative permeability using pore-network modeling, Transp. Porous Media. 74 (2008) 201–219. doi:10.1007/s11242-007-9191-7.

[40] K.S. Sra, N.R. Thomson, M. Asce, J.F. Barker, Persulfate Treatment of Dissolved Gasoline Compounds, J. Hazardous, Toxic, Radioact. Waste. 17 (2013) 9–15. doi:10.1061/(ASCE)HZ.2153-5515.0000143.

[41] S.C. Ayirala, C.S. Vijapurapu, D.N. Rao, Beneficial effects of wettability altering surfactants in oil-wet fractured reservoirs, J. Pet. Sci. Eng. 52 (2006) 261–274. doi:10.1016/j.petrol.2006.03.019.

[42] L.N. Nwidee, M. Lebedev, A. Barifcani, M. Sarmadivaleh, S. Iglauer, Wettability alteration of oil-wet limestone using surfactant-nanoparticle formulation, J. Colloid Interface Sci. 504 (2017) 334–345. doi:10.1016/j.jcis.2017.04.078.

[43] Y. Tsai, F. Chou, S. Cheng, Using tracer technique to study the flow behavior of surfactant foam, J. Hazard. Mater. 166 (2009) 1232–1237. doi:10.1016/j.jhazmat.2008.12.038.

552 [44] W.R. Rossen, Theory of Mobilization Pressure Gradient of Flowing Foams in Porous Media, J.
553 Colloid Interface Sci. 136 (1990) 1–16. doi:10.1016/0021-9797(90)90074-X.

554 [45] S. Jeong, S.E. Roosevelt, Micromodel Study of Surfactant Foam Remediation of Residual
555 Trichloroethylene, Envirenmental Sci. Technol. 34 (2000) 3456–3461. doi:10.1021/es9910558.

556 [46] S. Wang, C.N. Mulligan, An evaluation of surfactant foam technology in remediation of
557 contaminated soil, Chemosphere. 57 (2004) 1079–1089.
558 doi:10.1016/j.chemosphere.2004.08.019.

559 [47] T. Robert, R. Martel, R. Lefebvre, J.M. Lauzon, A. Morin, Impact of heterogeneous properties
560 of soil and LNAPL on surfactant-enhanced capillary desaturation, J. Contam. Hydrol. 204
561 (2017) 57–65. doi:10.1016/j.jconhyd.2017.07.006.

562 [48] C. Liang, H. Su, Identification of Sulfate and Hydroxyl Radicals in Thermally Activated
563 Persulfate, Ind. Eng. Chem. Res. 48 (2009) 5558–5562. doi:10.1021/ie9002848.

564 [49] H. Liu, T.A. Bruton, F.M. Doyle, D.L. Sedlak, In situ chemical oxidation of contaminated
565 groundwater by persulfate: Decomposition by Fe(III)- and Mn(IV)-containing oxides and
566 aquifer materials, Environ. Sci. Technol. 48 (2014) 10330–10336. doi:10.1021/es502056d.

567 [50] P. Shukla, S.K. Upadhyay, Kinetics of oxidation of non-ionic surfactants (Triton X-100 and Brij-
568 35) by KMnO4 in H2SO4 medium, Indian J. Chem. 47 (2008) 1037–1040.

569 [51] C. Trellu, N. Oturan, Y. Pechaud, E.D. Van Hullebusch, G. Esposito, M.A. Oturan, Anodic
570 oxidation of surfactants and organic compounds entrapped in micelles - Selective degradation
571 mechanisms and soil washing solution reuse, Water Res. 118 (2017) 1–11.
572 doi:10.1016/j.watres.2017.04.013.

573

12 injection experiments:

3 oxidant delivery fluids

2 contamination contrasts

2 permeability contrasts